Dynamically-Orthogonal Parabolic Equations for Probabilistic Ocean Acoustics in the New England Seamounts

M.M.N. Robin[a,b], P.J. Haley, Jr.[a], C. Mirabito[a], and P.F.J. Lermusiaux[a,†]
[a]*Department of Mechanical Engineering, Massachusetts Institute of Technology, Cambridge, MA*
[b] *Mines Paris PSL, France*
[†]Corresponding author: pierrel@mit.edu

***Abstract*—Underwater sound propagation is sensitive to specific environmental features and specific operational configuration parameters. We illustrate the preliminary use of our deterministic and stochastic Dynamically-Orthogonal Wide-Angle Parabolic Equations (DO-WAPEs) to classify and quantify the effects of ocean uncertainties and source depth uncertainties on the acoustic fields. We showcase initial results for the New England Seamounts off the northeastern US coastline, emphasizing the effects of uncertain source depths and subsurface ocean inflows and acoustic ducts. The stochastic DO-WAPEs predict the probability distribution of the acoustic pressure and transmission loss fields. The mean and standard deviation of the TL field are described and linked to the ocean environment and seamount geometry. Mutual information is predicted to identify the TL locations most informative about the source depth.**

***Index Terms*—Underwater sound propagation, probabilistic forecasting, acoustics sensitivity, source-receiver configurations, DO-WAPE, Gulf Stream, New England Seamounts.**

I. Introduction

Underwater sound propagation is sensitive to specific features, scales, and gradients in the ocean environment, from turbulent processes at acoustic wavelengths to large-scale circulations at basin scales [1–3]. However, because of the limited ocean observations, wide range of scales, and dynamic ocean processes, it is challenging to model and predict all these acoustics-relevant ocean features at sufficient levels of accuracy. In addition, the dominant sensitivities are themselves not always well known or understood [4, 5], especially for strongly nonlinear effects. Finally, acoustic sensitivities depend on the sound frequency, source-receiver configuration, and many other operational and environmental factors. To further scientific understanding and augment acoustics modeling capabilities, both process studies of nonlinear sensitivities and stochastic modeling are useful. The former enables targeted studies of complex processes using data and models, while the latter augments deterministic modeling with probabilistic environmental conditions and stochastic forcing inputs. The results can capture the environmental inputs that matter and organize them by their acoustic importance, both dynamically and probabilistically [6, 7].

In this work, we illustrate the preliminary use of our deterministic [8] and stochastic Dynamically-Orthogonal Parabolic Equations (DO-ParEq) [9–13] to classify and quantify the effects of ocean uncertainties and source depth uncertainties on the acoustic fields. As our probabilistic acoustics characterization is organized by variance [14–18], we can estimate ocean variability and operational configurations that lead to the largest variance in underwater sound pressure fields. We report initial results for the New England Seamounts off the northeastern US coastline in the Atlantic Ocean. We also illustrate how one could use our DO-ParEq to identify the features of ocean fields and operational configurations that are most informative, in the sense of mutual information [19–21], about underwater sound propagation. A long-term goal is to utilize our nonlinear stochastic DO analysis to quantify acoustics dynamical regimes and complete global dynamical analyses of ocean acoustics sensitivity [7, 19, 22, 23].

The New England Seamounts are a chain of seamounts located southeast of Georges Bank. The oceanography of the deep water is dominated by the Gulf Stream (separating the colder, fresher slope water mass from the warmer, saltier Sargasso water mass) and the rings it sheds [24–28]. The Gulf Stream passes through this chain, which affects its stability [29] and the characteristics of its rings [30]. On the shelf, the overall flow is to the southwest, starting from Baffin Bay to the north and ending to the south at Cape Hatteras [31]. Tides also play an important role on the shelf, especially in the Bay of Fundy [32, 33] and in the strong tidal rectification around Georges Bank [34–36]. Around the seamounts, barotropic tides are much weaker than in shallower coastal regions such as Georges Bank and the Gulf of Maine, but internal tides and waves occur [37, 38]. Figure (1a) shows an estimate of the 50 m sound speed field in this Gulf Stream and New England Seamounts region, overlaid with current vectors, for 0Z on July 5, 2024 [39]. Figure (1b) shows the local bathymetry and the location for the acoustic section shown in Figure (2).

The present probabilistic ocean acoustics work was developed in preparation for the New England Seamount Acoustic (NESMA) collaborative sea experiment in the New England Seamount Chain. An Intensive Observation Period (IOP) for NESMA occurred in July 2024 [39]. Before and during this NESMA IOP, we employed the MIT-MSEAS (Multidisciplinary Simulation, Estimation, and Assimilation Systems) to simulate and predict the ocean and underwater acoustic fields. For the ocean, we utilize our MIT-MSEAS data-assimilative Primitive-Equation (PE) submesoscale-to-regional-scale ocean-modeling system [40, 41], initialized by downscaling from global models and with data corrections. Our ocean ensemble forecasts are initialized with 3D PE-field perturbations from Error Subspace Statistical Estimation

OCEANS 2024 - Halifax | 979-8-3315-4008-1/24/$31.00 ©2024 IEEE | DOI: 10.1109/OCEANS55160.2024.10754458

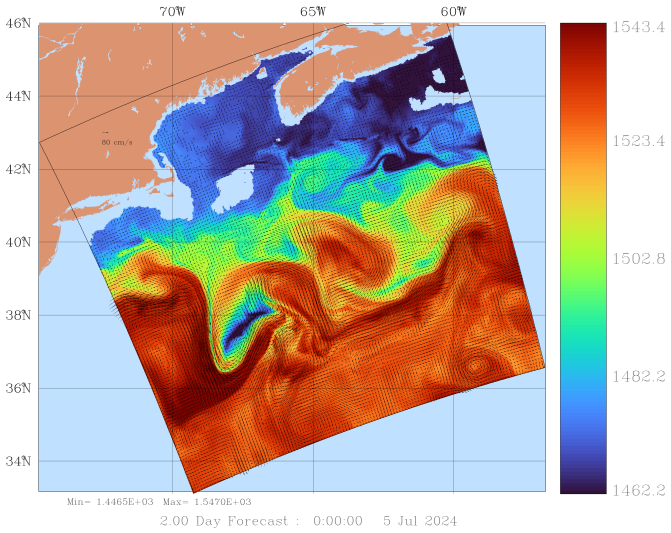

(a) 50 m sound speed field (m/s)

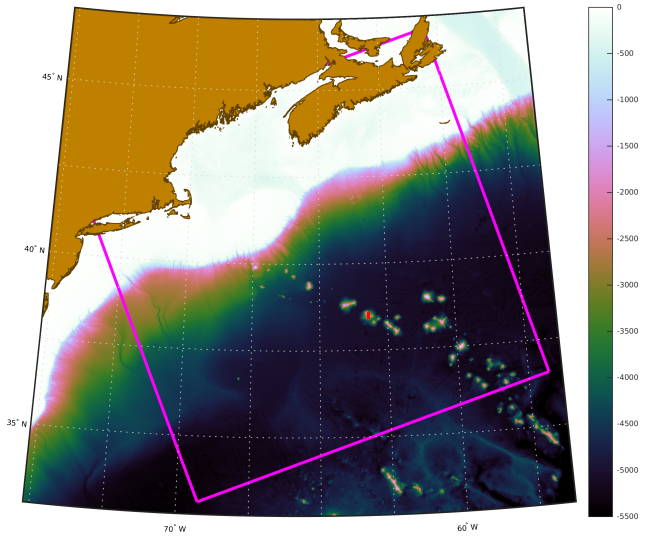

(b) Domain and bathymetry (m)

Fig. 1: MIT-MSEAS ocean modeling for the New England Seamounts. (a) 50 m sound speed overlaid with current vectors, as forecast by our ocean primitive-equation system for 0Z on July 5, 2024; (b) Simulation domain and bathymetry. The red line denotes the location of the north-south DO-ParEq computational section (30 km long) illustrated in Figure (3).

(ESSE) [20, 22, 42–44] and forced with stochastic tides and air-sea fluxes [21, 45]. These probabilistic forecasts of ocean sound speed and density fields are then used as inputs to our acoustic modeling, specifically the MIT-MSEAS deterministic ParEq and stochastic DO-ParEq systems.

In what follows, in Section II, we describe our integrated stochastic ocean physics and stochastic acoustics methodology. In Section III, we exemplify the preliminary results of our deterministic and probabilistic ocean acoustics predictions in the New England Seamounts region. We emphasize the effects of uncertain source depths, subsurface ocean inflows, and acoustic ducts. Finally, we conclude in Section IV.

II. Methodology

A. Ocean Physics

For ocean physics simulations, we employ the MIT-MSEAS ocean modeling system. The main system is based on a nonlinear free-surface hydrostatic primitive-equation model [40, 41]. It uses second-order structured finite volumes and is configured with generalized-level vertical coordinates and implicit two-way nesting. The MSEAS primitive-equation can simulate (sub)-mesoscale processes over nested domains with complex geometries and varied interactions, using an implicit two-way nesting/tiling. We can incorporate varied subsystems into a particular instance of the MSEAS primitive-equation solver including initialization schemes [41], nested tidal prediction and inversion [46], fast-marching coastal objective analysis [47], subgrid-scale models [6, 44], biogeochemical models [48–50], and advanced data assimilation [22, 51]. MSEAS has been applied to ocean monitoring [52] and ecosystem prediction and environmental management [53–56]. Directly relevant to present effort is the use of MSEAS for ocean-acoustic uncertainty quantification and data assimilation [57–66].

B. Ocean Acoustics

For ocean acoustics, we employ our deterministic and stochastic acoustics Padé-WAPE models. Considering an acoustic modeling domain, we denote the physical position as $\boldsymbol{x} = (\boldsymbol{x}_\perp, \eta)$, where $\boldsymbol{x}_\perp$ denotes the two-dimensional transverse coordinates and η the position in the range direction. In general, the ocean environment is uncertain such that the sound speed, density, attenuation, and acoustic fields are all uncertain and thus stochastic: the sound speed field $c = c(\boldsymbol{x}_\perp, \eta; \xi)$, density field $\rho = \rho(\boldsymbol{x}_\perp, \eta; \xi)$, attenuation coefficient field $a = a(\boldsymbol{x}_\perp, \eta; \xi)$, and outgoing complex-valued acoustic field $\boldsymbol{\psi} = \boldsymbol{\psi}(\boldsymbol{x}_\perp, \eta; \xi)$ all depend on ξ, the realization parameter. Therefore, the Padé-WAPE is generalized to the following stochastic PDE [8, 11, 67]:

$$\frac{\partial}{\partial \eta}\boldsymbol{\psi}(\boldsymbol{x}_\perp, \eta; \xi) = ik_0 \sum_{k=1}^{n_p} \left(\mathbf{I} + b_{k,n_p}\mathbf{X}(\boldsymbol{x}_\perp, \eta; \xi)\right)^{-1} a_{k,n_p}\mathbf{X}(\boldsymbol{x}_\perp, \eta; \xi)\,\boldsymbol{\psi}(\boldsymbol{x}_\perp, \eta; \xi)\,, \quad (1)$$

where n_p is the number of Padé series terms, and a_{k,n_p} and b_{k,n_p} for $1 \le k \le n_p$ are real coefficients given by

$$a_{k,n_p} = \frac{2}{2n_p+1}\sin^2\left(\frac{k\pi}{2n_p+1}\right) \quad \text{and} \quad b_{k,n_p} = \cos^2\left(\frac{k\pi}{2n_p+1}\right). \quad (2)$$

In addition, the stochastic differential operator $\mathbf{X}(\boldsymbol{x}_\perp, \eta; \xi)$ encodes the uncertainties in the stochastic squared effective index of refraction n^2_{eff}, defined respectively as

$$\mathbf{X}(\boldsymbol{x}_\perp, \eta; \xi) = \frac{1}{k_0^2}\nabla^2_\perp + \left(n^2_{eff}(\boldsymbol{x}_\perp, \eta; \xi) - 1\right)\mathbf{I}\,. \quad (3)$$

and, using ρ for $\rho(\boldsymbol{x}_\perp, \eta; \xi)$,

$$n^2_{eff}(\boldsymbol{x}_\perp, \eta; \xi) = \left(\frac{c_0}{c(\boldsymbol{x}_\perp, \eta; \xi)}\right)^2\left(1 + i\frac{a(\boldsymbol{x}_\perp, \eta; \xi)}{27.29}\right) + \frac{1}{2k_0^2}\left(\frac{1}{\rho}\nabla^2\rho - \frac{3}{2\rho^2}|\nabla\rho|^2\right). \quad (4)$$

If we fix the realization parameter ξ, the above Padé-WAPE (1) is deterministic and we can use our MSEAS-ParEq system [8]. It solves several versions of the Padé-WAPE [1, 68, 69]. It uses second-order spatial finite volume (FV) schemes for the transverse space operators and high-order range marching schemes. It is initialized by analytical starters [1] and self-starters [70, 71]. The solvers employ efficient dimension-splitting techniques for propagation in large domains and have been validated on several benchmark cases [72, 73].

If we solve the stochastic Padé-WAPE system for many realizations ξ, we employ the Dynamically Orthogonal (DO) decomposition [9, 10, 15, 16, 18, 74, 75]. The DO theory and schemes were used to derive instantaneously-optimal range-dynamic stochastic reduced-order equations. With DO schemes, the stochastic fields of the effective index of refraction $n^2_{eff}(\boldsymbol{x}_\perp, \eta; \xi)$ and the complex envelope pressure component $\boldsymbol{\psi}^{(k)}(\boldsymbol{x}_\perp, \eta; \xi)$ for $1 \le k \le n_p$ are decomposed as

$$n^2_{eff}(\boldsymbol{x}_\perp, \eta; \xi) \approx \left(n^2_{eff}\right)_{DO} = \overline{n^2}(\boldsymbol{x}_\perp, \eta) + \sum_{l=1}^{n_{s,n^2}} \widetilde{n^2}_l(\boldsymbol{x}_\perp, \eta)\, \beta_l(\eta; \xi)\ , \tag{5a}$$

$$\boldsymbol{\psi}^{(k)}(\boldsymbol{x}_\perp, \eta; \xi) \approx \boldsymbol{\psi}^{(k)}_{DO} = \overline{\boldsymbol{\psi}}^{(k)}(\boldsymbol{x}_\perp, \eta) + \sum_{i=1}^{n_{s,\boldsymbol{\psi}}} \widetilde{\boldsymbol{\psi}}^{(k)}_i(\boldsymbol{x}_\perp, \eta)\, \alpha^{(k)}_i(\eta; \xi)\ , \tag{5b}$$

where $\overline{n^2}(\boldsymbol{x}_\perp, \eta)$ and $\overline{\boldsymbol{\psi}}^{(k)}(\boldsymbol{x}_\perp, \eta)$ are the statistical mean fields for the index of refraction and complex pressure component, respectively. The fields $\widetilde{n^2}_l(\boldsymbol{x}_\perp, \eta)$ for $l = 1, \ldots, n_{s,n^2}$ and $\widetilde{\boldsymbol{\psi}}^{(k)}_i(\boldsymbol{x}_\perp, \eta)$ for $i = 1, \ldots, n_{s,\boldsymbol{\psi}}$ are DO modes that form orthonormal range-dynamic bases for the index of refraction and complex pressure component, respectively. The DO stochastic coefficients $\beta_l(\eta; \xi)$ for $l = 1, \ldots, n_{s,n^2}$ and $\alpha^{(k)}_i(\eta; \xi)$ for $i = 1, \ldots, n_{s,\boldsymbol{\psi}}$ are each zero-mean stochastic processes.

The DO methodology [9–11, 67] then proceeds to obtain range-dynamic differential equations for the mean $\overline{\boldsymbol{\psi}}^{(k)}(\boldsymbol{x}_\perp, \eta)$, DO modes $\widetilde{\boldsymbol{\psi}}^{(k)}_i(\boldsymbol{x}_\perp, \eta)$, and stochastic DO coefficients $\alpha^{(k)}_i(\eta; \xi)$:

$$\frac{\partial \overline{\boldsymbol{\psi}}^{(k)}(\boldsymbol{x}_\perp, \eta)}{\partial \eta} = \mathbb{E}^\xi\left[\mathcal{L}_{WAPE}\left[\boldsymbol{\psi}^{(k)}(\boldsymbol{x}_\perp, \eta; \xi); \xi\right]\right], \tag{6a}$$

$$\frac{\partial \widetilde{\boldsymbol{\psi}}^{(k)}_i(\boldsymbol{x}_\perp, \eta)}{\partial \eta} = \sum_{j=1}^{n_{s,\boldsymbol{\psi}}} C^{-1}_{\alpha_i\alpha_j} \Pi^\perp_{\overline{\boldsymbol{\psi}}} \mathbb{E}^\xi\left[\mathcal{L}_{WAPE}\left[\boldsymbol{\psi}^{(k)}(\boldsymbol{x}_\perp, \eta; \xi); \xi\right] \alpha^{(k)}_j(\eta; \xi)\right], \tag{6b}$$

$$\frac{d\alpha^{(k)}_i(\eta; \xi)}{d\eta} = \left\langle \mathcal{L}_{WAPE}\left[\boldsymbol{\psi}^{(k)}(\boldsymbol{x}_\perp, \eta; \xi); \xi\right] - \mathbb{E}^\xi\left[\mathcal{L}_{WAPE}\left[\boldsymbol{\psi}^{(k)}(\boldsymbol{x}_\perp, \eta; \xi); \xi\right]\right], \widetilde{\boldsymbol{\psi}}^{(k)}_i(\boldsymbol{x}_\perp, \eta)\right\rangle, \tag{6c}$$

where $1 \le k \le n_p$ is the Padé index, $\mathcal{L}_{WAPE}$ is the stochastic WAPE operator here written as [11, 67]

$$\mathcal{L}_{WAPE} = ik_0\left(a_{k,n_p}\mathbf{X}(\boldsymbol{x}_\perp, \eta; \xi) - a_{k,n_p}b_{k,n_p}\mathbf{X}^2(\boldsymbol{x}_\perp, \eta; \xi)\right)\boldsymbol{\psi}^{(k)}(\boldsymbol{x}_\perp, \eta; \xi)\ , \tag{7}$$

$C_{\alpha_i\alpha_j}$ are range-dependent covariance functions defined as

$$C_{\alpha_i\alpha_j}(\eta) = \mathbb{E}^\xi\left[\alpha^{(k)}_i(\eta; \xi)\, \alpha^{(k)}_j(\eta; \xi)\right], \tag{8}$$

and $\Pi^\perp_{\widetilde{\boldsymbol{\psi}}}$ is a projection operator onto a space orthogonal to the stochastic DO subspace

$$\Pi^\perp_{\widetilde{\boldsymbol{\psi}}}[v] = v - \sum_{i=1}^{n_{s,\boldsymbol{\psi}}} \left\langle v, \widetilde{\boldsymbol{\psi}}^{(k)}_i(\boldsymbol{x}_\perp, \eta)\right\rangle \widetilde{\boldsymbol{\psi}}^{(k)}_i(\boldsymbol{x}_\perp, \eta)\ , \tag{9}$$

where v is a spatial field in the transverse space.

The DO-WAPE initial conditions, boundary conditions, numerical schemes, Padé integrations, and implementation are similar to the DO-NAPE and are discussed in [9, 11, 67]. We also refer to these references for additional details and definitions. As part of the present work, we evaluated our DO-WAPE schemes and implementation using an idealized seamount test case [11, 67] and augmented the DO-WAPE software to enable the present realistic seamount application.

III. Applications

We now apply our MSEAS ocean physics modeling system and deterministic and probabilistic ocean acoustics models to the New England Seamounts region.

During the real-time experiment [39], our MSEAS ocean forecasts were commonly 3 to 4 days in duration, using 100 optimized vertical levels and 2.4 km horizontal resolution. Initial conditions were downscaled from two global models (HYCOM and Mercator) and corrected using some data of opportunity. They were forced by blended atmospheric flux field forecasts from the High-Resolution Window (HIRESW) 5 km Model and Global Forecast System (GFS) 0.25° model from the National Centers for Environmental Prediction (NCEP), and by tides from TPXO9-Atlas of OSU adapted to the higher-resolution bathymetry and coastlines [46]. We utilized a bathymetry blended from the Shuttle Radar Topography Mission (SRTM) 15-arcsecond global map [76] and the 1-arcsecond NOAA coastal relief bathymetry [77]. Forecast fields were issued daily and described using snapshot time-series maps, sections, and interactive visualization [78]. The data of opportunity and data from NESMA were processed and displayed (Argo float and glider CTDs, NDBC buoy data, and satellite SSH and SST), see [39]. We used these data to evaluate the skill of our forecasts in real time, computing skill metrics based on differences between measured values and forecasts at data points.

To initialize the ESSE ocean ensemble forecast, we segregated the historical June/July/August CTD profiles (2000–2023) from the World Ocean Database [79] into six water mass regions. Horizontal correlations for the deep water had a 150 km decay scale and 375 km zero-crossing while the shelf had 100 km decay scale and 250 km zero-crossing. Initial velocity perturbations were computed using a 4000 m level of

no motion. These perturbations were then applied to central initial condition and boundary condition fields, downscaled from Mercator or HYCOM. To simulate the uncertainty in the ocean forcings, we tune and apply small random amplitude/phase perturbations to the deterministic atmospheric and tidal forcings, leading to stochastic ocean forcing [44].

In what follows, we illustrate our acoustic modeling in preparation for the NESMA sea experiment and present preliminary probabilistic ocean acoustics modeling using ocean fields before observations from the IOP were assimilated.

A. Deterministic WAPE Simulations

Figure (2) illustrates sound propagation across the Atlantis II Seamount at 0Z on March 11, 2024. On that day, the Gulf Stream is impinging on Atlantis II, as visible in the sound speed section (Fig. 2a). A sound speed minimum is present at depths of about 500 m to 1000 m, with a slope from left to right. Intrusions of colder waters from the shelf and slope off Nova Scotia are also estimated in the upper layers, from about 50 to 200 m depths. Using the MSEAS-ParEq model [8], we simulate sound propagation from a sound source at 910 m depth and frequency of 550 Hz (Fig. 2b). The transmission loss (TL) curve versus range at a receiver depth of 910 m shows the decay in energy received before the seamount, an increase at the seamount, and then a variation with range past the seamount in response to the ocean features (Fig. 2a). The TL highlights the effects of the seamount and sound-channel variability, redirecting sound energy in the upward-sloping sound channel past the seamount. In the upper ocean layers, acoustic ducts are also simulated to occur at several depths mostly within 50 to 200 m, enabling shallower transmission and sound trapping over significant distances.

B. Stochastic DO-WAPE: Sensitivity to Source Depth

We now consider the effects of uncertain source depths on underwater sound propagation across the Atlantis II Seamount. Our MSEAS forecast of sound speed across the Atlantis II Seamount in a north-south section of 30 km range for 0Z on July 5, 2024, is shown in Figure (3). The upper 500 m sound speed field highlights cold water inflows from the shelf and slope off Nova Scotia from 50 m to about 150 m north of the seamount (right side of the panels) as well as the warmer surface layer sloping down to the south (left slide of panels). It also predicts some cooler filaments of about 5 to 10 m thickness at shallow depths (around 10 to 50 m). The full sound speed field shows the sound channel from 500 to 1500 m depth, with a range-dependent minimum sound speed at depths of 600 to 800 m and of variable thickness.

For the stochastic acoustics, we employ our DO-WAPE modeling. The north-south DO-WAPE computational domain is the 30 km section whose ocean environment is illustrated in Fig. (3) and location in Fig. (1b). The source frequency f is 550 Hz. It is located at the southernmost edge of the computational domain, at the left side of Fig. (3). The source depth is uncertain with a uniform probability distribution between 50 and 110 m. To represent this uncertainty, a total

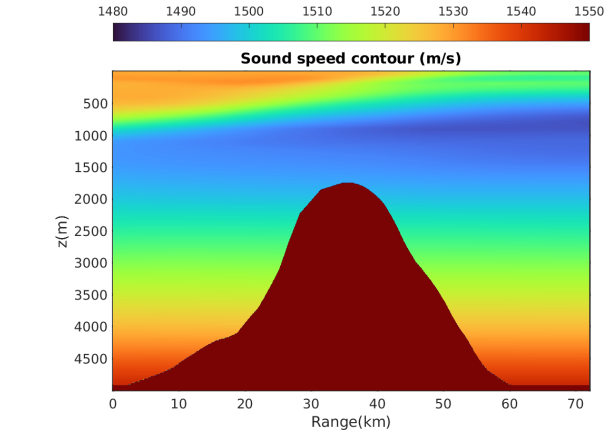

(a) Sound speed vertical section (m/s)

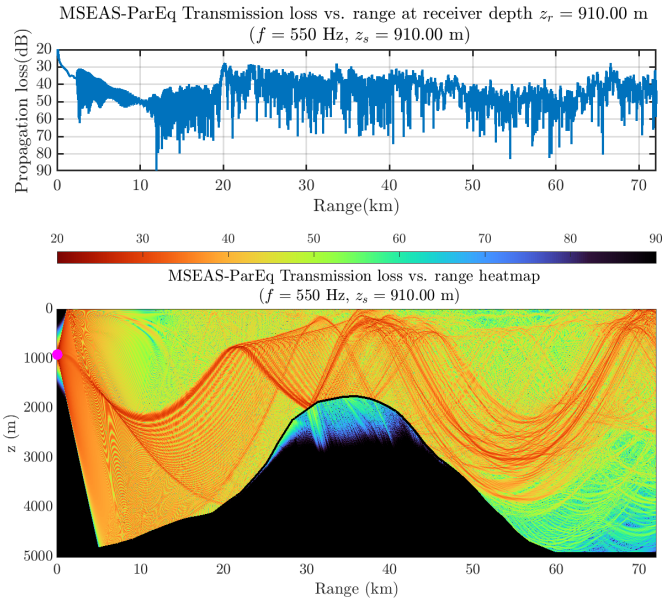

(b) Transmission Loss (TL) field (dB) for a source depth of 910 m and 550 Hz frequency. Cylindrical spreading was removed from TL.

Fig. 2: MIT-MSEAS sound propagation simulation around the Atlantis II Seamount at 0Z on March 11, 2024. The cooler and sloping sound channel (a), due in part to the slope water affects the TL curve and field (b, right side). When combined with seamount effects, it leads to upward-sloping acoustic rays and upward-sloping mid-depth minima in TL. Upper-layer acoustic ducts are also observed within depths of about 50 to 200 m.

of $n_{r,\boldsymbol{\psi}} = 2000$ realizations is employed for the source depth and corresponding stochastic DO coefficients of $\boldsymbol{\psi}$. The size of the stochastic DO subspace for $\boldsymbol{\psi}$ was tuned to $n_{s,\boldsymbol{\psi}} = 40$, and the number of Padé series terms in the DO-WAPE solution was set to $n_p = 15$. The numerical spatial grid is discretized with $dz = 1$ m and $d\eta = 2$ m. The computational saving in using the DO-WAPE methodology instead of direct Monte Carlo simulations is of the order of $2000/40 = 50$.

Figure (4) illustrates some of the results of our numerical integration of the stochastic DO-WAPE (6a-c). Specifically, Figure (4a) shows the statistical mean TL field from 500 m to 30 km range as obtained from the reconstructed DO re-

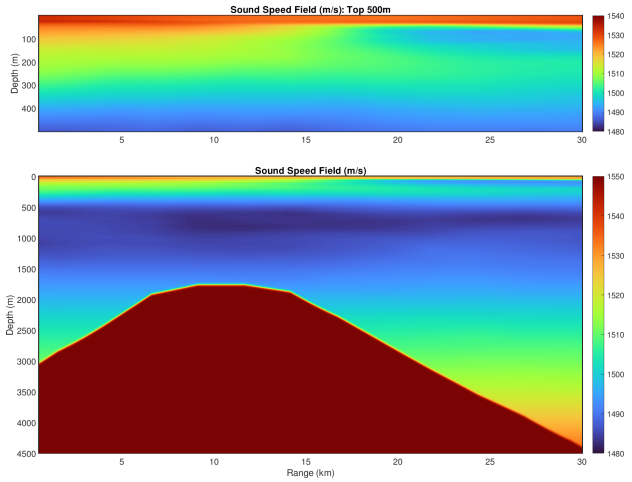

Fig. 3: MIT-MSEAS forecast sound speed field (m/s) for the Atlantis II Seamount at 0Z on July 5, 2024. The top panel is a zoom to the upper 500 m; the bottom panel shows the full section. The 30 km section location is illustrated in Fig. (1b).

alizations of ψ while Figure (5a) shows the corresponding statistical standard deviation of the TL field. As expected, the mean TL field is much smoother than the 2000 TL realizations reconstructed for the DO decomposition of ψ (not shown). It nonetheless highlights shallow acoustic ducts and enhanced subsurface propagation past the seamount from about 50 m to 250 m depth. In response to the uncertain source depth, the TL standard deviation field predicts the highest variations ($\pm$16 dB) for the edges of the dominant rays, especially for the steeper direct rays to the seamount. The reflected rays past the seamount also show high deviations, especially for the returning sound energy from surface bounces ($\pm$12 dB).

Next, we use our DO-WAPE uncertainty quantification and information theory to estimate where the source depth affects the TL field the most, given the seamount geometry and the simulated sound speed field. Motivating questions include how does acoustics dynamics transform the probability distribution of the source depth, and which TL location provides the most information about the source depth. We compute mutual information (MI) between variables as MI generalizes covariance and correlation concepts to non-Gaussian probability distributions and vector variables [19].

Figure (5) illustrates the predicted MI field between the depth of the sound source and the TL values in the section. The MI field indicates the TL locations most informative about the source depths, and vice versa. The most informative locations seem to be governed by a combination of uncertainty (standard deviation) and reflections. For ranges smaller than the top of the seamount, TL does not discriminate the original source depth well. After the top of the seamount, there is a beam of strong MI that tracks well with a similar beam in the standard deviation, even fading out around 20 km range (where the standard deviation beam also fades). In this beam, the higher variability coupled with the details of the reflection renders the TL a good discriminator of source depth. After 20 km, a

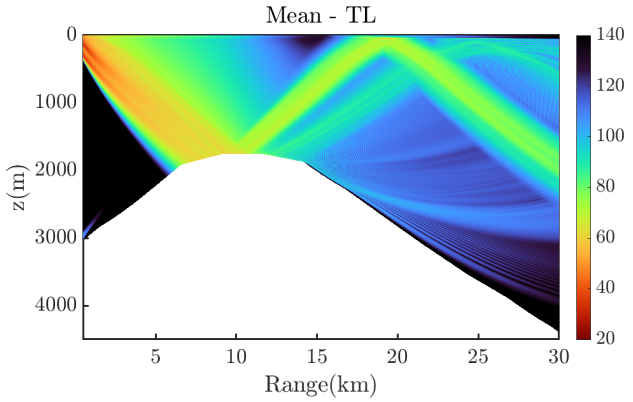

(a) MSEAS DO-WAPE TL Mean field (dB)

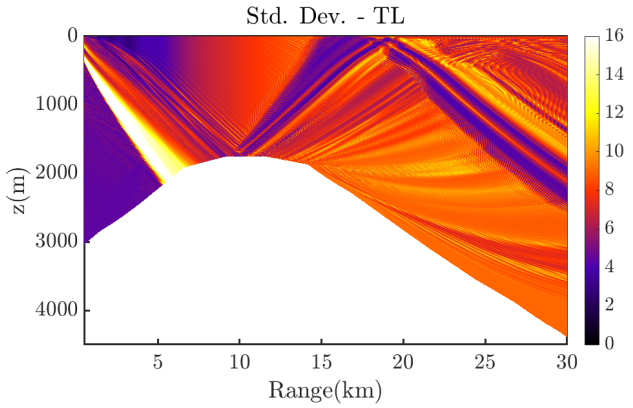

(b) MSEAS DO-WAPE TL Standard Deviation field (dB)

Fig. 4: MIT-MSEAS stochastic DO-WAPE simulations for the Atlantis II Seamount at 0Z on July 5, 2024. (a) Statistical mean TL field, as obtained from the DO-WAPE decomposition of ψ. (b) Statistical standard deviation TL field, as predicted using the DO-WAPE. The location of the 30 km section is illustrated in Fig. (1b).

second strong beam of MI tracks a similar strong beam of standard deviation reflecting from the surface.

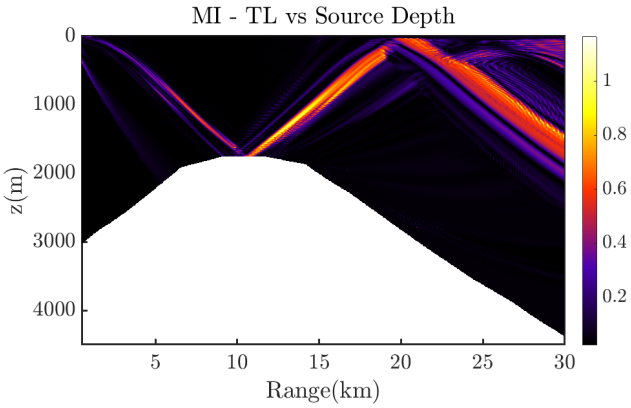

(a) MSEAS DO-WAPE MI field between TL and Source Depth

Fig. 5: Mutual Information between TL and sound source depth, computed from the MIT-MSEAS stochastic DO-WAPE simulations for the Atlantis II Seamount on 0Z, July 5, 2024. Again, the section location is illustrated in Fig. (1b).

IV. Conclusions

In this paper, we described preliminary deterministic and stochastic Dynamically-Orthogonal Parabolic Equations (DO-ParEq) simulations to classify and quantify the effects of source depth uncertainties on underwater acoustic fields. We showcased initial results for the New England Seamounts off the eastern US coastline. The stochastic DO-WAPEs are used to predict the probability distribution of the acoustic pressure and transmission loss fields. The mean and standard deviation of the TL field are described and linked to the ocean environment and seamount geometry. Mutual information is predicted to identify the TL locations most informative about the source depth.

Our preliminary simulations indicate that the DO-ParEq approach is a promising technique for classifying the environmental inputs that matter most for specific source-receiver parameters and configurations. In the future, one could study the sensitivity to different source-receiver configurations (source/receiver depths, their separation, their number, etc.), source frequency and spectrum, and ocean features and dynamics (Gulf Stream state, eddy field, subsurface filaments, etc.). In general, we can utilize the DO-ParEq to simulate, decompose, and characterize the acoustic responses to variability and stochasticity in the ocean features, seabed characteristics, and operational acoustics parameters such as source depths, ranges, and frequencies.

Acknowledgments

We thank all members of the MSEAS group. We are grateful to the Task Force Ocean (TFO) program under the Office of Naval Research (ONR) for partial research support under grant N00014-19-1-2664 (DEEP-AI) to the Massachusetts Institute of Technology (MIT). We also thank all members of the New England Seamount Acoustic (NESMA) team, especially Dr. Y.-T. Lin, the chief scientist, and Dr. Robert Todd for the glider collaboration. We thank the HYCOM Consortium and Mercator Ocean for their ocean model fields and NCEP for their atmospheric forcing forecasts.

References

[1] F. B. Jensen, W. A. Kuperman, M. B. Porter, and H. Schmidt, *Computational ocean acoustics*. Springer Science & Business Media, 2011.

[2] A. Tolstoy, "3-D propagation issues and models," *Journal of Computational Acoustics*, vol. 04, no. 03, pp. 243–271, 1996.

[3] P. C. Etter, *Underwater acoustic modeling and simulation*. CRC press, 2018.

[4] T. F. Duda and B. D. Cornuelle, "Summary of acoustics-in-focus panel discussion special session "underwater sound modeling: Comprehensive environmental descriptions"," in *Proceedings of Meetings on Acoustics*, vol. 43, no. 1. AIP Publishing, 2021.

[5] E. K. Skarsoulis and B. D. Cornuelle, "Travel-time sensitivity kernels in ocean acoustic tomography," *The Journal of the Acoustical Society of America*, vol. 116, no. 1, pp. 227–238, 2004.

[6] P. F. J. Lermusiaux, "Evolving the subspace of the three-dimensional multiscale ocean variability: Massachusetts Bay," *Journal of Marine Systems*, vol. 29, no. 1, pp. 385–422, 2001.

[7] T. P. Sapsis, M. P. Ueckermann, and P. F. J. Lermusiaux, "Global analysis of Navier–Stokes and Boussinesq stochastic flows using dynamical orthogonality," *Journal of Fluid Mechanics*, vol. 734, pp. 83–113, 2013.

[8] W. H. Ali, A. Charous, C. Mirabito, P. J. Haley, Jr., and P. F. J. Lermusiaux, "MSEAS-ParEq for ocean-acoustic modeling around the globe," in *OCEANS 2023 IEEE/MTS Gulf Coast*. Biloxi, MS: IEEE, Sep. 2023.

[9] W. H. Ali and P. F. J. Lermusiaux, "Dynamically orthogonal narrow-angle parabolic equations for stochastic underwater sound propagation. part I: Theory and schemes," *Journal of the Acoustical Society of America*, vol. 155, no. 1, pp. 640–655, Jan. 2024.

[10] ——, "Dynamically orthogonal narrow-angle parabolic equations for stochastic underwater sound propagation. part II: Applications," *Journal of the Acoustical Society of America*, vol. 155, no. 1, pp. 656–672, Jan. 2024.

[11] ——, "Dynamically orthogonal wide-angle parabolic equations for stochastic underwater sound propagation," *Journal of the Acoustical Society of America*, 2024, in preparation.

[12] A. Charous and P. F. J. Lermusiaux, "Dynamically orthogonal differential equations for stochastic and deterministic reduced-order modeling of ocean acoustic wave propagation," in *OCEANS 2021 IEEE/MTS*. IEEE, Sep. 2021, pp. 1–7.

[13] ——, "Range-dynamical low-rank split-step Fourier method for the parabolic wave equation," *Journal of the Acoustical Society of America*, 2024, sub-judice.

[14] P. F. J. Lermusiaux, C.-S. Chiu, G. G. Gawarkiewicz, P. Abbot, A. R. Robinson, R. N. Miller, P. J. Haley, Jr, W. G. Leslie, S. J. Majumdar, A. Pang, and F. Lekien, "Quantifying uncertainties in ocean predictions," *Oceanography*, vol. 19, no. 1, pp. 92–105, 2006.

[15] F. Feppon and P. F. J. Lermusiaux, "Dynamically orthogonal numerical schemes for efficient stochastic advection and Lagrangian transport," *SIAM Review*, vol. 60, no. 3, pp. 595–625, 2018.

[16] ——, "A geometric approach to dynamical model-order reduction," *SIAM Journal on Matrix Analysis and Applications*, vol. 39, no. 1, pp. 510–538, 2018.

[17] A. Charous and P. F. J. Lermusiaux, "Dynamically orthogonal Runge–Kutta schemes with perturbative retractions for the dynamical low-rank approximation," *SIAM Journal on Scientific Computing*, vol. 45, no. 2, pp. A872–A897, 2023.

[18] ——, "Stable rank-adaptive dynamically orthogonal Runge–Kutta schemes," *SIAM Journal on Scientific Computing*, vol. 46, no. 1, pp. A529–A560, 2024.

[19] P. F. J. Lermusiaux, D. N. Subramani, J. Lin, C. S. Kulkarni, A. Gupta, A. Dutt, T. Lolla, P. J. Haley, Jr., W. H. Ali, C. Mirabito, and S. Jana, "A future for intelligent autonomous ocean observing systems," *Journal of Marine Research*, vol. 75, no. 6, pp. 765–813, Nov. 2017, the Sea. Volume 17, The Science of Ocean Prediction, Part 2.

[20] P. F. J. Lermusiaux, P. J. Haley, Jr., S. Jana, A. Gupta, C. S. Kulkarni, C. Mirabito, W. H. Ali, D. N. Subramani, A. Dutt, J. Lin, A. Shcherbina, C. Lee, and A. Gangopadhyay, "Optimal planning and sampling predictions for autonomous and Lagrangian platforms and sensors in the northern Arabian Sea," *Oceanography*, vol. 30, no. 2, pp. 172–185, Jun. 2017, special issue on Autonomous and Lagrangian Platforms and Sensors (ALPS).

[21] P. F. J. Lermusiaux, P. J. Haley, Jr., C. Mirabito, E. M. Mule *et al.*, "Real-time ocean probabilistic forecasts, reachability analysis, and adaptive sampling in the Gulf of Mexico," in *OCEANS 2024 IEEE/MTS Halifax*. Halifax: IEEE, Sep. 2024, in press.

[22] P. F. J. Lermusiaux, "Adaptive modeling, adaptive data assimilation and adaptive sampling," *Physica D: Nonlinear Phenomena*,

vol. 230, no. 1, pp. 172–196, 2007.
[23] P. Lu and P. F. J. Lermusiaux, "Bayesian learning of stochastic dynamical models," *Physica D: Nonlinear Phenomena*, vol. 427, p. 133003, Dec. 2021.
[24] A. Gangopadhyay, G. Gawarkiewicz, E. N. S. Silva, A. M. Silver, M. Monim, and J. Clark, "A census of the warm-core rings of the gulf stream: 1980–2017," *Journal of Geophysical Research: Oceans*, vol. 125, no. 8, p. e2019JC016033, 2020.
[25] A. Gangopadhyay, G. Gawarkiewicz, E. N. S. Silva, M. Monim, and J. Clark, "An observed regime shift in the formation of warm core rings from the gulf stream," *Scientific reports*, vol. 9, no. 1, p. 12319, 2019.
[26] A. Silver, A. Gangopadhyay, G. Gawarkiewicz, A. Taylor, and A. Sanchez-Franks, "Forecasting the gulf stream path using buoyancy and wind forcing over the north atlantic," *Journal of Geophysical Research: Oceans*, vol. 126, no. 8, p. e2021JC017614, 2021, e2021JC017614 2021JC017614. [Online]. Available: https://agupubs.onlinelibrary.wiley.com/doi/abs/10.1029/2021JC017614
[27] A. Silver, A. Gangopadhyay, G. Gawarkiewicz, E. N. S. Silva, and J. Clark, "Interannual and seasonal asymmetries in gulf stream ring formations from 1980 to 2019," *Scientific Reports*, vol. 11, no. 2207, 2021. [Online]. Available: https://doi.org/10.1038/s41598-021-81827-y
[28] A. Silver, A. Gangopadhyay, G. Gawarkiewicz, P. Fratantoni, and J. Clark, "Increased gulf stream warm core ring formations contributes to an observed increase in salinity maximum intrusions on the northeast shelf," *Scientific Reports*, vol. 13, no. 7538, 2023.
[29] E. P. Chassignet, X. Xu, A. Bozec, and T. Uchida, "Impact of the new england seamount chain on gulf stream pathway and variability," *Journal of Physical Oceanography*, vol. 53, no. 8, pp. 1871 – 1886, 2023. [Online]. Available: https://journals.ametsoc.org/view/journals/phoc/53/8/JPO-D-23-0008.1.xml
[30] A. Silver, A. Gangopadhyay, G. Gawarkiewicz, M. Andres, G. Flierl, and J. Clark, "Spatial variability of movement, structure, and formation of warm core rings in the northwest atlantic slope sea," *Journal of Geophysical Research: Oceans*, vol. 127, no. 8, p. e2022JC018737, 2022, e2022JC018737 2022JC018737. [Online]. Available: https://agupubs.onlinelibrary.wiley.com/doi/abs/10.1029/2022JC018737
[31] J. W. Loder, "The coastal ocean off northeastern north america: A large-scale view," *The sea*, vol. 11, pp. 105–138, 1998.
[32] C. Garrett, "Tidal resonance in the bay of fundy and gulf of maine," *Nature*, vol. 238, no. 5365, pp. 441–443, 1972. [Online]. Available: https://doi.org/10.1038/238441a0
[33] B. S. David A. Greenberg, Wade Blanchard and E. Barrow, "Climate change, mean sea level and high tides in the bay of fundy," *Atmosphere-Ocean*, vol. 50, no. 3, pp. 261–276, 2012. [Online]. Available: https://doi.org/10.1080/07055900.2012.668670
[34] J. W. Loder and D. G. Wright, "Tidal rectification and frontal circulation on the sides of georges bank," *Journal of Marine Research 43*, no. 3, 1985. [Online]. Available: https://elischolar.library.yale.edu/journal_of_marine_research/1788
[35] J. W. Loder, K. F. Drinkwater, N. S. Oakey, E. P. W. Horne, J. M. Huthnance, B. S. McCartney, D. Prandle, H. Charnock, K. R. Dyer, J. M. Huthnance, P. S. Liss, J. H. Simpson, and P. B. Tett, "Circulation, hydrographic structure and mixing at tidal fronts: the view from Georges Bank," *Philosophical Transactions of the Royal Society of London. Series A: Physical and Engineering Sciences*, vol. 343, no. 1669, pp. 447–460, 1993.
[36] D. R. Lynch, C. E. Naimie, J. T. Ip, C. V. Lewis, F. E. Werner, R. A. Luettich Jr, B. O. Blanton, J. Quinlan, D. J. McGillicuddy Jr, J. R. Ledwell *et al.*, "Real-time data assimilative modeling on georges bank," *Oceanography*, vol. 14, no. SPL. ISS. 1, pp. 65–77, 2001.
[37] S. M. Kelly and P. F. J. Lermusiaux, "Internal-tide interactions with Gulf Stream and Middle Atlantic Bight shelfbreak front," *Journal of Geophysical Research: Oceans*, vol. 121, pp. 6271–6294, 2016.
[38] S. M. Kelly, P. F. J. Lermusiaux, T. F. Duda, and P. J. Haley, Jr., "A coupled-mode shallow water model for tidal analysis: Internal-tide reflection and refraction by the Gulf Stream," *Journal of Physical Oceanography*, vol. 46, pp. 3661–3679, 2016.
[39] MSEAS NESMA Ex., "New England Seamounts Experiment Acoustics (NESMA) 2024: New England Seamount Chain – July, 2024," Jul. 2024. [Online]. Available: http://mseas.mit.edu/Sea_exercises/NESMA/
[40] P. J. Haley, Jr. and P. F. J. Lermusiaux, "Multiscale two-way embedding schemes for free-surface primitive equations in the "Multidisciplinary Simulation, Estimation and Assimilation System"," *Ocean Dynamics*, vol. 60, no. 6, pp. 1497–1537, Dec. 2010.
[41] P. J. Haley, Jr., A. Agarwal, and P. F. J. Lermusiaux, "Optimizing velocities and transports for complex coastal regions and archipelagos," *Ocean Modelling*, vol. 89, pp. 1–28, May 2015.
[42] P. F. J. Lermusiaux and A. R. Robinson, "Data assimilation via Error Subspace Statistical Estimation, part I: Theory and schemes," *Monthly Weather Review*, vol. 127, no. 7, pp. 1385–1407, 1999.
[43] P. F. J. Lermusiaux, "Data assimilation via Error Subspace Statistical Estimation, part II: Mid-Atlantic Bight shelfbreak front simulations, and ESSE validation," *Monthly Weather Review*, vol. 127, no. 7, pp. 1408–1432, Jul. 1999.
[44] P. F. J. Lermusiaux, "Uncertainty estimation and prediction for interdisciplinary ocean dynamics," *Journal of Computational Physics*, vol. 217, no. 1, pp. 176–199, 2006.
[45] P. J. Haley, Jr., C. Mirabito, M. Doshi, and P. F. J. Lermusiaux, "Ensemble forecasting for the Gulf of Mexico Loop Current region," in *OCEANS 2023 IEEE/MTS Gulf Coast*. Biloxi, MS: IEEE, Sep. 2023.
[46] O. G. Logutov and P. F. J. Lermusiaux, "Inverse barotropic tidal estimation for regional ocean applications," *Ocean Modelling*, vol. 25, no. 1–2, pp. 17–34, 2008. [Online]. Available: http://www.sciencedirect.com/science/article/pii/S1463500308000851
[47] A. Agarwal and P. F. J. Lermusiaux, "Statistical field estimation for complex coastal regions and archipelagos," *Ocean Modelling*, vol. 40, no. 2, pp. 164–189, 2011.
[48] P. F. J. Lermusiaux, P. J. Haley, W. G. Leslie, A. Agarwal, O. Logutov, and L. J. Burton, "Multiscale physical and biological dynamics in the Philippine Archipelago: Predictions and processes," *Oceanography*, vol. 24, no. 1, pp. 70–89, 2011, Special Issue on the Philippine Straits Dynamics Experiment.
[49] P. F. J. Lermusiaux, C. Evangelinos, R. Tian, P. J. Haley, Jr, J. J. McCarthy, N. M. Patrikalakis, A. R. Robinson, and H. Schmidt, "Adaptive coupled physical and biogeochemical ocean predictions: A conceptual basis," in *Computational Science - ICCS 2004*, ser. Lecture Notes in Computer Science. Springer Berlin Heidelberg, 2004, vol. 3038, pp. 685–692.
[50] C. Evangelinos, R. Chang, P. F. J. Lermusiaux, and N. M. Patrikalakis, "Rapid real-time interdisciplinary ocean forecasting using adaptive sampling and adaptive modeling and legacy codes: Component encapsulation using XML," in *Computational Science–ICCS 2003*. Springer, 2003, pp. 375–384.
[51] P. F. J. Lermusiaux, "Estimation and study of mesoscale variability in the Strait of Sicily," *Dynamics of Atmospheres and Oceans*, vol. 29, no. 2, pp. 255–303, 1999.
[52] P. F. J. Lermusiaux, P. J. Haley, Jr, and N. K. Yilmaz, "Environmental prediction, path planning and adaptive sampling: Sensing and modeling for efficient ocean monitoring, management and pollution control," *Sea Technology*, vol. 48, no. 9, pp. 35–38,

2007.
[53] Ş. T. Beşiktepe, P. F. J. Lermusiaux, and A. R. Robinson, "Coupled physical and biogeochemical data-driven simulations of Massachusetts Bay in late summer: Real-time and post-cruise data assimilation," *Journal of Marine Systems*, vol. 40–41, pp. 171–212, 2003.
[54] G. Cossarini, P. F. J. Lermusiaux, and C. Solidoro, "Lagoon of Venice ecosystem: Seasonal dynamics and environmental guidance with uncertainty analyses and error subspace data assimilation," *Journal of Geophysical Research: Oceans*, vol. 114, no. C6, Jun. 2009.
[55] A. Gupta, P. J. Haley, D. N. Subramani, and P. F. J. Lermusiaux, "Fish modeling and Bayesian learning for the Lakshadweep Islands," in *OCEANS 2019 MTS/IEEE SEATTLE*. Seattle: IEEE, Oct. 2019, pp. 1–10.
[56] P. J. Haley, Jr., A. Gupta, C. Mirabito, and P. F. J. Lermusiaux, "Towards Bayesian ocean physical-biogeochemical-acidification prediction and learning systems for Massachusetts Bay," in *OCEANS 2020 IEEE/MTS*. IEEE, Oct. 2020, pp. 1–9.
[57] P. F. J. Lermusiaux and C.-S. Chiu, "Four-dimensional data assimilation for coupled physical-acoustical fields," in *Acoustic Variability, 2002*, N. G. Pace and F. B. Jensen, Eds. Saclantcen: Kluwer Academic Press, 2002, pp. 417–424.
[58] P. F. J. Lermusiaux, C.-S. Chiu, and A. R. Robinson, "Modeling uncertainties in the prediction of the acoustic wavefield in a shelfbreak environment," in *Proceedings of the 5th International Conference on Theoretical and Computational Acoustics*, E.-C. Shang, Q. Li, and T. F. Gao, Eds. World Scientific Publishing Co., May 21-25 2002, pp. 191–200, refereed invited manuscript.
[59] A. R. Robinson and P. F. J. Lermusiaux, "Prediction systems with data assimilation for coupled ocean science and ocean acoustics," in *Proceedings of the Sixth International Conference on Theoretical and Computational Acoustics*, A. Tolstoy et al, Ed. World Scientific Publishing, 2004, pp. 325–342, refereed invited Keynote Manuscript.
[60] P. F. J. Lermusiaux, P. J. Haley, Jr., C. Mirabito, W. H. Ali, M. Bhabra, P. Abbot, C.-S. Chiu, and C. Emerson, "Multi-resolution probabilistic ocean physics-acoustic modeling: Validation in the New Jersey continental shelf," in *OCEANS 2020 IEEE/MTS*. IEEE, Oct. 2020, pp. 1–9.
[61] P. F. J. Lermusiaux, C. Mirabito, P. J. Haley, Jr., W. H. Ali, A. Gupta, S. Jana, E. Dorfman, A. Laferriere, A. Kofford, G. Shepard, M. Goldsmith, K. Heaney, E. Coelho, J. Boyle, J. Murray, L. Freitag, and A. Morozov, "Real-time probabilistic coupled ocean physics-acoustics forecasting and data assimilation for underwater GPS," in *OCEANS 2020 IEEE/MTS*. IEEE, Oct. 2020, pp. 1–9.
[62] J. Xu, P. F. J. Lermusiaux, P. J. Haley Jr., W. G. Leslie, and O. G. Logutov, "Spatial and Temporal Variations in Acoustic propagation during the PLUSNet-07 Exercise in Dabob Bay," in *Proceedings of Meetings on Acoustics (POMA)*, vol. 4. Acoustical Society of America 155th Meeting, 2008, p. 11.
[63] F.-P. A. Lam, P. J. Haley, Jr., J. Janmaat, P. F. J. Lermusiaux, W. G. Leslie, M. W. Schouten, L. A. te Raa, and M. Rixen, "At-sea real-time coupled four-dimensional oceanographic and acoustic forecasts during Battlespace Preparation 2007," *Journal of Marine Systems*, vol. 78, no. Supplement, pp. S306–S320, Nov. 2009.
[64] P. F. J. Lermusiaux, J. Xu, C.-F. Chen, S. Jan, L. Chiu, and Y.-J. Yang, "Coupled ocean–acoustic prediction of transmission loss in a continental shelfbreak region: Predictive skill, uncertainty quantification, and dynamical sensitivities," *IEEE Journal of Oceanic Engineering*, vol. 35, no. 4, pp. 895–916, Oct. 2010.
[65] T. F. Duda, Y.-T. Lin, W. Zhang, B. D. Cornuelle, and P. F. J. Lermusiaux, "Computational studies of three-dimensional ocean sound fields in areas of complex seafloor topography and active ocean dynamics," in *Proceedings of the 10th International Conference on Theoretical and Computational Acoustics*, Taipei, 2011.
[66] M. E. G. D. Colin, T. F. Duda, L. A. te Raa, T. van Zon, P. J. Haley, Jr., P. F. J. Lermusiaux, W. G. Leslie, C. Mirabito, F. P. A. Lam, A. E. Newhall, Y.-T. Lin, and J. F. Lynch, "Time-evolving acoustic propagation modeling in a complex ocean environment," in *OCEANS - Bergen, 2013 MTS/IEEE*, 2013, pp. 1–9.
[67] W. H. Ali, "Stochastic dynamically orthogonal modeling and Bayesian learning for underwater acoustic propagation," Ph.D. dissertation, Massachusetts Institute of Technology, Department of Mechanical Engineering and Computational Science and Engineering, Cambridge, Massachusetts, Sep. 2023.
[68] F. Sturm and J. A. Fawcett, "On the use of higher-order azimuthal schemes in 3-d pe modeling," *JASA*, vol. 113, no. 6, pp. 3134–3145, 2003.
[69] J. F. Claerbout, *Fundamentals of geophysical data processing*. Citeseer, 1985.
[70] M. D. Collins, "A self-starter for the parabolic equation method," *The Journal of the Acoustical Society of America*, vol. 92, no. 4, pp. 2069–2074, 10 1992.
[71] ——, "The stabilized self-starter," *The Journal of the Acoustical Society of America*, vol. 106, no. 4, pp. 1724–1726, 10 1999.
[72] W. H. Ali, M. S. Bhabra, P. F. J. Lermusiaux, A. March, J. R. Edwards, K. Rimpau, and P. Ryu, "Stochastic oceanographic-acoustic prediction and Bayesian inversion for wide area ocean floor mapping," in *OCEANS 2019 MTS/IEEE SEATTLE*. Seattle: IEEE, Oct. 2019, pp. 1–10.
[73] W. H. Ali, "Dynamically orthogonal equations for stochastic underwater sound propagation," Master's thesis, Massachusetts Institute of Technology, Computation for Design and Optimization Program, Cambridge, Massachusetts, Sep. 2019.
[74] T. P. Sapsis and P. F. J. Lermusiaux, "Dynamically orthogonal field equations for continuous stochastic dynamical systems," *Physica D: Nonlinear Phenomena*, vol. 238, no. 23–24, pp. 2347–2360, Dec. 2009.
[75] ——, "Dynamical criteria for the evolution of the stochastic dimensionality in flows with uncertainty," *Physica D: Nonlinear Phenomena*, vol. 241, no. 1, pp. 60–76, 2012.
[76] B. Tozer *et al.*, "Global bathymetry and topography at 15 arc sec: SRTM15+," *Earth and Space Science*, vol. 6, no. 10, pp. 1847–1864, 2019.
[77] NOAA National Centers for Environmental Information, "Coastal relief models (CRMs) [data set]," 2023, Accessed 2024-05-13. [Online]. Available: https://doi.org/10.25921/5ZN5-KN44
[78] W. H. Ali, M. H. Mirhi, A. Gupta, C. S. Kulkarni, C. Foucart, M. M. Doshi, D. N. Subramani, C. Mirabito, P. J. Haley, Jr., and P. F. J. Lermusiaux, "Seavizkit: Interactive maps for ocean visualization," in *OCEANS 2019 MTS/IEEE SEATTLE*. Seattle: IEEE, Oct. 2019, pp. 1–10.
[79] T. P. Boyer *et al.*, *World Ocean Database 2018*, NOAA, Silver Spring, MD, 2018.